

Chapter 2 *Synthesis and Characterization Techniques*

2.1 Sample preparation

Various strategies have been used to synthesise MnO₂ nanostructures with various controllable morphologies (shape and size), surface area and porosity, which are crucial for determining the properties of MnO₂. Microwave, co-precipitation, reflux root, electrochemical deposition, and hydrothermal methods are used for the synthesis of nanostructured MnO₂. Among these methods, hydrothermal technique is one of the simpler, facile and one step method for synthesizing nanoparticles without the need of surfactant/template. This technique does not require high-temperature annealing of the samples for a long time period as required in other techniques like sol-gel, coprecipitation and so on. This not only add up the fabrication cost but it also degrades the reproducibility as in case of hydrothermal technique. The particle grows slowly under hydrothermal conditions, which are regulated by modulating reaction parameters such as temperature, pressure, dwell period, reagent concentration, and solvents employed in the reaction. Owing to these merits of hydrothermal method over alternative chemical techniques, in this work, we have used this method to synthesise various polymorphs of MnO₂. α , β , δ and mixed phase of α and β MnO₂ along with Dy doped α -MnO₂ have been synthesized by means of hydrothermal technique which is explained below.

2.1.1 Hydrothermal Synthesis Technique

(a) α -, β - and $\alpha\beta$ - MnO_2 nanorods

For the synthesis of α - MnO_2 , Manganese sulphate (MnSO_4 , 98%, Merk) and Potassium permanganate (KMnO_4 , 98.5%, Merk) were dissolved in distilled water in initial molar ratio of 2:3 to form a solution. To form a complete dissolution of chemical reagents, the solution was mixed properly with the help of magnetic stirrer at room temperature. Further, the homogenous solution was transferred to a Teflon lined stainless steel autoclave and heated at 160°C for 12 h. Afterwards, the vessel was allowed to cool naturally to room temperature. The dark brown precipitate settled at the bottom of the vessel was collected and centrifuged several times using distilled water followed by ethanol. Finally, the precipitate was dried in a vacuum oven at 80°C for 12 hours and the fine powder was formed after grinding it thoroughly in a mortar and pestle. The schematic diagram for the synthesis of MnO_2 is shown in figure 2.1. Chemical reaction used to synthesize MnO_2 nanostructures is described as follows



One can tune several phases of MnO_2 by varying the concentration of potassium permanganate in the above solution. More the content of potassium permanganate, more open is the structure. On increasing the concentration of KMnO_4 , the β phase of MnO_2 has been transformed to α phase and then δ phase of MnO_2 . For α - MnO_2 nanorods, the initial molar ratio of $\text{KMnO}_4/\text{MnSO}_4$ was 2:3 with equal molarity. On changing the molarity of KMnO_4 from 1M to 0.1M, an intermediate γ - MnOOH phase was formed. When the solution was placed in an autoclave with stirring for 12 h, a mixture of two phases, α - MnO_2

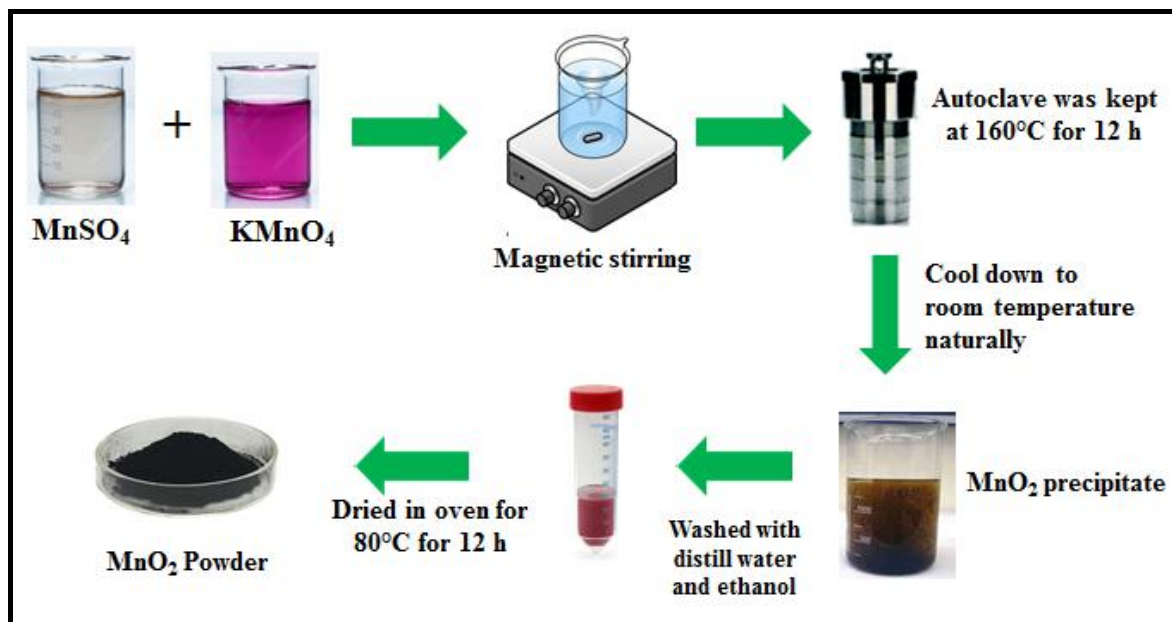


Figure 2.1: Flow chart for the synthesis of MnO₂ using hydrothermal technique.

and β -MnO₂ were obtained, denoted as $\alpha\beta$ -MnO₂. As obtained samples were dried in an oven and further calcined at 400°C for 4 h in a furnace in the presence of air. After annealing, no change in structure of α and $\alpha\beta$ -MnO₂ was observed except in γ -MnOOH which transform to β -MnO₂. The flow chart of parameters required for the synthesis α -, β -, and $\alpha\beta$ -MnO₂ samples is shown in figure 2.2.

(b) δ -MnO₂

For the synthesis of δ -MnO₂, the homogeneous solution of KMnO₄/MnSO₄ was made with initial molar ratio of 6:1 with equal molarity. The solution was placed in an autoclave and heated for 120°C for 6 h. The rest of the process for synthesis is same as illustrated above. The schematic diagram of hydrothermal parameters required for the synthesis of δ -MnO₂ is shown in figure 2.3.

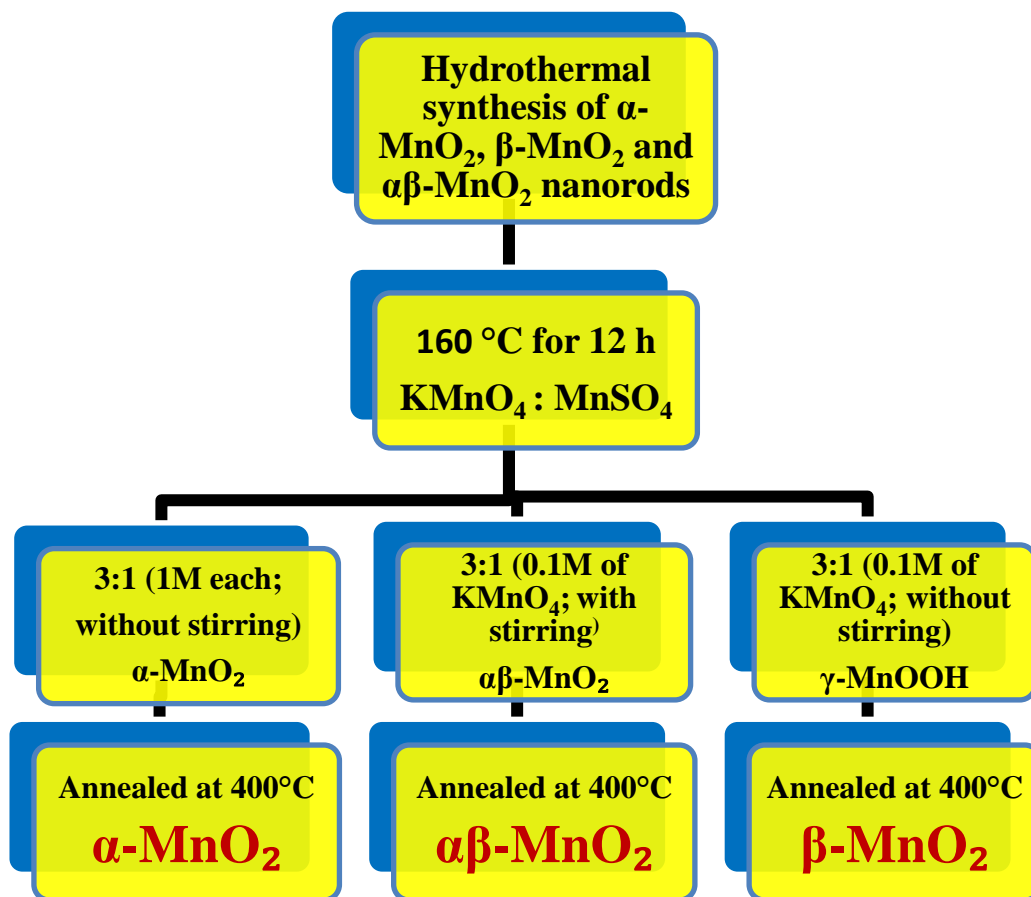


Figure 2.2: Flow chart for the Synthesis of α -MnO₂, β -MnO₂, and $\alpha\beta$ -MnO₂.

(c) α -MnO₂ and Dy doped α -MnO₂ nanorods

Pure and Dy doped α -MnO₂ nanorods were synthesised with varying Dy concentrations using hydrothermal synthesis technique at 120°C. In a typical procedure, an appropriate amount of Potassium permanganate (KMnO₄, 98.5%, Merk), Manganese sulphate (MnSO₄.H₂O, 98%, Merk) and different mol percentage of Dysprosium nitrate (Dy (NO₃)₃.xH₂O, 99.99%, Sigma Aldrich) 0, 5, 10, 15 and 20 mol% were dissolved into 230 ml of distilled water under vigorous stirring. After the formation of homogenous

solution of chemical reagents, obtained mixture was transferred into a 300 ml Teflon (PTFE) lined stainless steel autoclave and heated at 120°C for 8 h. The vessel was allowed to cool to room temperature naturally. A dark brown precipitate settled at the bottom of an autoclave was collected by filtering and washing several times with deionized water and ethanol. Finally, the products were dried at 80°C in vacuum oven for 12 h. Further, it was converted into powder after grinded in an agate mortar and pestle. Flow chart for the synthesis of Pure and Dy doped α -MnO₂ nanorods are shown in figure 2.3 and 2.4, respectively.

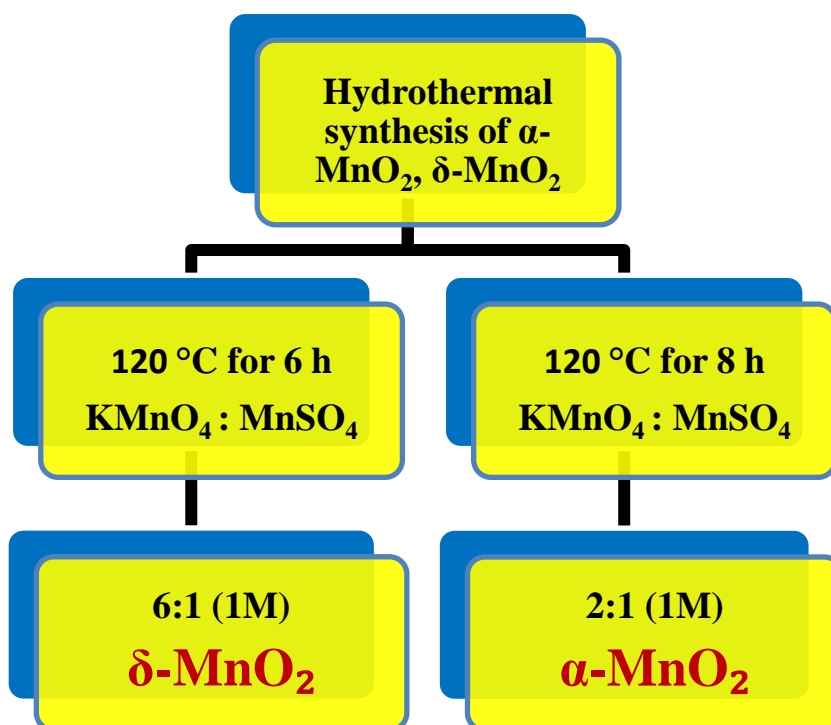


Figure 2.3: Flow chart for the Synthesis of δ -MnO₂ and α -MnO₂.

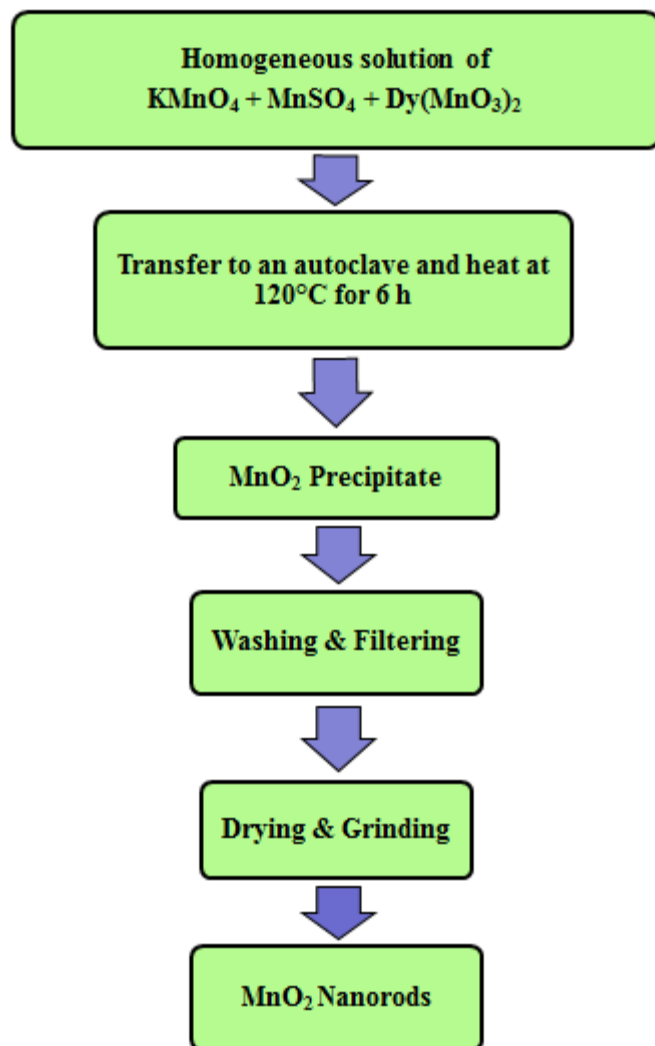


Figure 2.4: Schematic Flow chart for the synthesis of bare and Dy doped α -MnO₂.

2.2 Characterization Techniques

α -, β -, δ - phase of MnO₂ and Dy doped α -MnO₂ samples prepared through hydrothermal technique were characterized using suitable methods to explore structural, microstructural, optical, magnetic and electrochemical properties. All of the characterization techniques used in this work are concisely illustrated below.

2.2.1 X-ray Diffraction (XRD)

X-ray diffraction (XRD), a non-destructive method is the most frequently used technique primarily employed to investigate the purity as well as crystal structure of the material. It also gives information regarding the crystallite size, orientation of crystallites, strain etc. A beam of X-rays (electromagnetic wave) of wavelength $\sim 1.54 \text{ \AA}$, diffracted in different directions when it fall on a lattice planes of the crystalline material of definite structure. Because of the similar order of magnitude of the wavelengths of X-rays and crystal lattice, the crystal structure can be determined by quantifying the intensities and angle of the beams diffracted from the lattice planes oriented in various directions.

XRD operates on the basis of Bragg's law and for a given interplaner spacing 'd', provision for diffraction to occur is given by

$$2d_{hkl} \sin\theta = n\lambda \quad (2.2)$$

where, d_{hkl} is the interplanar spacing and h, k, l are the Miller indices, X-ray incident on the surface of the sample at some angle ' θ ' and, "n" is the integer (for XRD, $n=1$), and ' λ ' is the wavelength of the incident radiation [149]. This law states that the path difference between the rays diffracted from a set of equally spaced lattice planes is $n\lambda$. The diffracted rays interfere constructively. The schematic diagram of Bragg's law is shown in Figure 2.5. According to Bragg's law, X-rays diffracted from different planes of the lattice at a particular angle show the diffraction patterns of high intensity peaks. In general, the number of diffraction peaks depends on the symmetry of the structure; for example, crystals with low symmetry, such as monoclinic, show many diffraction peaks due to numerous lattice planes, whereas cubic and tetragonal crystals with specific lattice planes

show only a few diffraction peaks due to their high symmetry structure. The diffraction peaks and their intensities are also correlated with the dimension of particles in the crystal.

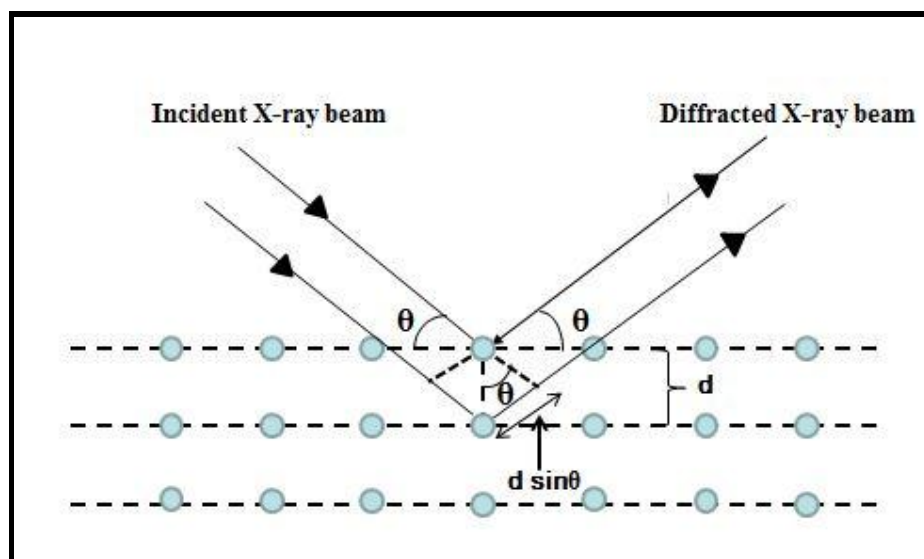


Figure 2.5: Schematic diagram of incident and diffracted X-rays from the crystal lattice.

Here, a rotating anode of 18 kW (CuK_α), Rigaku powder diffractometer operating with the Bragg-Brentano geometry which is fixed with a monochromator of graphite in the diffracted beam was used to record the diffraction patterns for the powder samples. This is the typical and suitable geometry for different material. During the XRD measurements of the powder samples, the current was 100 mA and the voltage was 40 kV with 2θ ranging from 10 to 90°. Samples with smooth surfaces are readily diffracted for data collection while using detector. Diffracted beams are measured into a count rate which is essentially converted by the detector. Finally, a plot including a succession of diffraction peaks as function of diffraction angle (2θ) is created, which is used to determine the crystallographic

information of the material. Schematic representation of X-ray technique is shown below (figure 2.6).

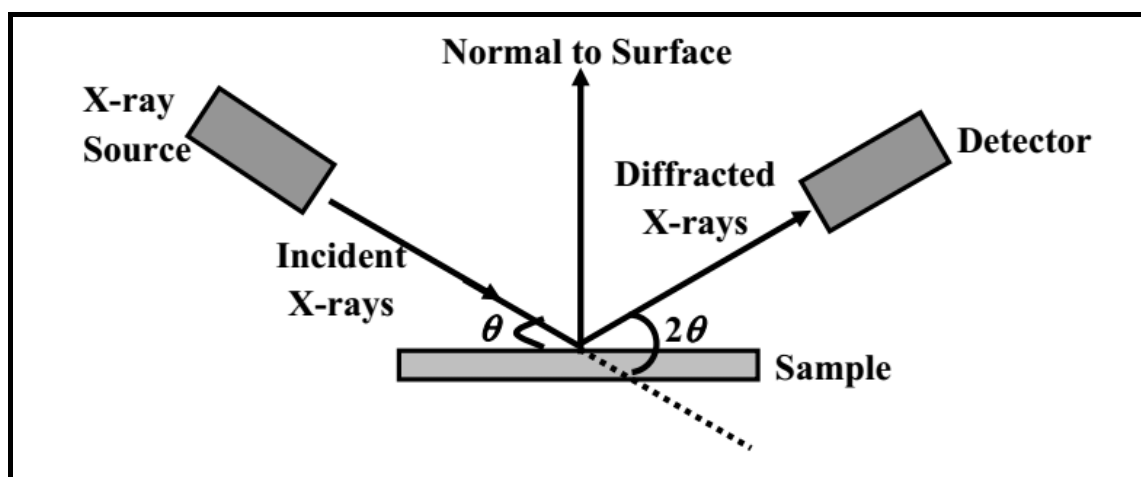


Figure 2.6: Schematic representation of X-ray technique.

In the present study, X-ray diffraction patterns were acquired using a Rigaku Miniflex X-ray diffractometer in Bragg-Brentano geometry with Cu K_{α} ($\lambda=1.54 \text{ \AA}$). The data from the Joint Committee on Powder Diffraction Standards is used to index XRD patterns (JCPDS). The crystallite size (D) was calculated using Scherrer equation [150] as written below

$$D = \frac{k\lambda}{\beta \cos\theta} \quad (2.3)$$

where, k is the Scherrer constant with a value of 0.9, λ is the wavelength of X-rays, β is FWHM (full width half maxima) and θ is the peak position in radian. Further, different structural data including atomic structure of a crystalline material, lattice constants, cell volume, bond lengths, and bond angles are recovered for synthesised materials using

Rietveld refinement of XRD patterns using FULLPROF programme. During refinement, pseudo-voigt function has been selected which have a combination of both Lorentzian and Gaussian distribution functions. The 6-coefficient polynomial function is considered as a background mode because the background data is found to be linear. The isotropic thermal parameter (B), occupancies are refined along with lattice parameter and atomic positions. The quality of the refinement is estimated from the χ^2 value which should be in between 0-1 for a good fit. This fitting method works by comparing the appropriate produced intensities to experimental data in order to find the crystal structure and other crystallographic information.

2.2.2 Fourier Transform Infrared Spectroscopy (FT-IR)

FT-IR is one the most common and widely used spectroscopic technique for the description of organic or inorganic molecules based on the presence of functional groups in the material. The term Fourier Transform Infrared Spectroscopy (FTIR) refers to a technological advancement in the collection and conversion of data from an interference pattern to a spectrum. FTIR is used to obtain emission or absorption spectrum of a molecule or an atom which occurs when atoms or molecules undergo transitions from one energy state to other.

The most important component used in FTIR spectrometer is Michelson interferometer. This interferometer is used to modulate the wavelength of infrared rays coming from electrically heated filament source. The filament is made of a combination of rare earth oxides. A grating made up of ATR or KBr which is transparent to infrared radiation are used to make the radiation monochromatic in nature. A detector detects transmitted or reflected radiations and recorded their intensity corresponding to each wavelength (λ). The

transmitted portion of the interferogram signals is sent to detector and analyzed using Fourier transform to obtain a single-beam IR spectrum. FTIR spectra are often displayed as intensity vs. wavenumber graphs (in cm^{-1}). The intensity of the spectrum can be plotted as light transmittance or absorbance at particular wavenumber. In this work, Thermo-Nicolet 5700 FT-IR was used to record the infrared spectra of MnO_2 samples in the range of 500 to 4000 cm^{-1} .

2.2.3 Raman spectroscopy

Raman spectroscopy is a non-destructive chemical evaluation method that offers precise information about the chemical structure, phase formation, and molecular interactions in the material. Both Raman and FTIR spectroscopy offer a spectrum characteristic of the unique vibrations of a molecule and are used to identify a material. Raman spectroscopy, on the other hand can provide additional information about lower frequency modes and vibrations that provides information about the crystal lattice or molecular structure.

Raman spectroscopy is a light scattering method that relies on light's interaction with chemical bonds inside a substance. A light coming from a high intensity laser source is scattered by the molecule. Most of the light scattered with wavelength as same the wavelength of the source as it scattered elastically. This is known as Rayleigh scattering or elastic scattering. However, the radiations scattered at different wavelengths has some loss or gain of energy, which depend on the chemical composition or crystallographic structure of the material. Such radiations are known as Raman scattering or inelastic scattering. In Raman scattering, the sample absorbs the photons from the laser light and re-emits it with shifted frequency. This shift exhibits the information regarding the rotational, vibrational as well as other low frequency transitions in molecules or solids.

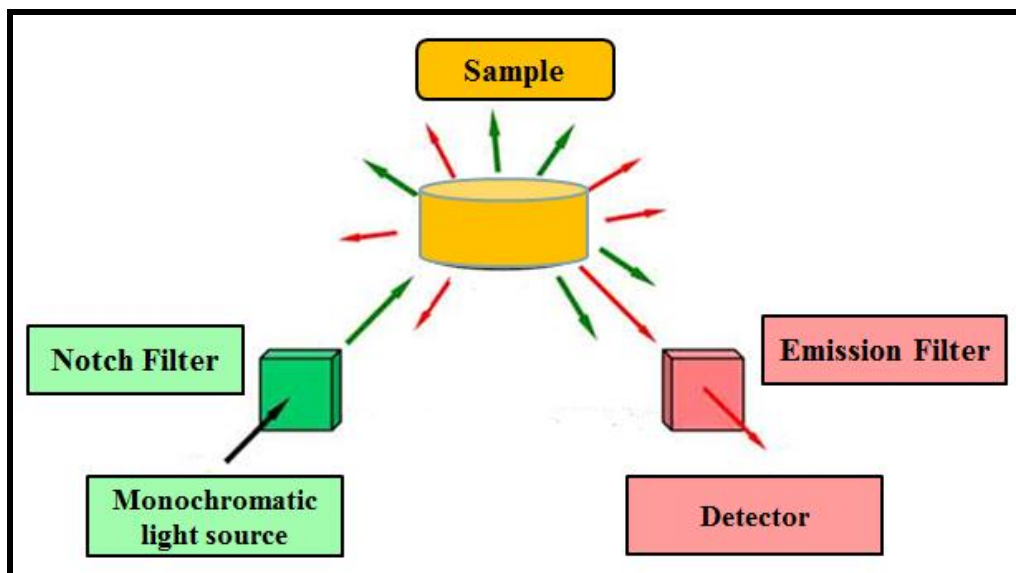


Figure 2.7: Schematic diagram for the simplified setup of Raman spectroscopy.

The experimental setup for Raman spectroscopy consists of a Raman spectrometer, measurement cell, and a detector is shown in figure 2.7. A laser source is used to incident a beam focused on a dichroic filter which reflects the beam to the sample at a 90° . The resulting scattered beam of same wavelength is focused back to the dichroic filter. Only the Raman scattered beam of a changed wavelength can pass through the filter without altering. Mirrors guide the measured light to a monochromator, which utilizes grating to diffract the beam into a narrow range of wavelengths. The photo current from each wavelength area is measured at the detector. Raman Spectrometer from Jobin Yvon Horiba (HR 800) and RENISHAW in Via consist of argon laser source of wavelength $\lambda \sim 488 \text{ nm}$ was used for the current work. Raman spectra of MnO_2 samples were recorded in between the 100 to 800 cm^{-1} .

2.2.4 Scanning Electron Microscope (SEM)

The topological and morphological information of the material is determined using a scanning electron microscope. It essentially shows the texture of the surfaces of the material. The electron beam is primarily incident on the surface of the sample and ionizes the atoms. As a result, the loosely bound electrons known as secondary electrons are ejected from such atoms. These secondary electrons have relatively low energy in the range of ~3 to 5 eV and can be easily identified. Such electrons are capable of creating the three dimensional image of the sample. A detector is used to collect these secondary electrons scattered from the sample and converts them into an electric signal after passing them through cathode ray oscilloscope (CRO). A high contrast image is formed on a screen of a computer. Using suitable detection mode, significant contrast against morphology is obtained. SEM has a spatial resolution of ~10 nm which allows it to resolve most of the surface characteristics.

Energy Dispersive X-ray Spectroscopy (EDS)

Energy Dispersive X-ray Spectroscopy (EDS or EDX) is a qualitative and quantitative X-ray microanalytical technique that provides information about the elemental composition of a compound. When we incident an electron beam on the surface of the sample it eject electrons. These ejected electrons create a vacancy in particular energy state which are filled by electrons from a higher state. When an electron from higher energy state comes to the lower energy state it emits photon in the form of x-ray and hence balances the energy difference between the two states. The energy of these emitted x-rays are the characteristic of the element. The detector is made up of a crystal that absorbs the expelled x-rays before measuring the relative quantity of released X-rays versus their energy.

For the present study, a high resolution emission gun based scanning electron microscope (HR-SEM) Zeiss (Germany), and Nova Nano SEM 450 of FEI make (USA, S.E.A) organized with the X-ray analyzer, were used. MnO₂ and Dy doped MnO₂ nanoparticles were mounted on the sample holder using carbon tape. The gun voltage was set to 5 kV and 15 kV in SE image mode to capture well focused images and energy dispersive spectra of the samples.

2.2.5 Transmission Electron Microscope (TEM)

Transmission Electron Microscopic technique (TEM) is a powerful technique for probing the structure and morphology including shape, size and distribution of nanoparticles. TEM comprises of an electron gun, a vacuum system, electromagnetic lenses, high voltage generator, recording devices and the associated electronics. The resolution of the modern TEM is under 0.2 nm even with a fair amount of the tilting of the specimen. TEM uses electrons of lower wavelength which makes it possible to get a high resolution image. A well-focused electron beam obtained from electron gun assembly and electromagnetic condenser lenses is accelerated by an anode, which is typically at 100 KeV with respect to the cathode. The beam is restricted by the condenser aperture, which stops un-collimated electrons. The collimated high energy (200 KeV and above) beam of electrons strikes the specimen and gets scattered depending upon the thickness and electron transparency of the specimen. The beam of scattered electron undergoing a change in phase and amplitude is focused by the objective lens which forms an image on phosphor screen or charge coupled device camera.

There are two basic modes of TEM operation: diffraction mode and imaging mode. In modern TEM, it is possible to switch from diffraction to imaging and vice-versa by changing the excitation of the lenses following the objective lens. The well distributed particles of TEM image could be analyzed for shape and size distribution. The histogram of particles distribution (particles size vs. number of particles) is plotted with the help of Image J software. Fitting of the data using Lorentzian distribution provides the average particle size. The selective area electron diffraction (SAED) pattern shows well concentric rings of different radii. The diffraction rings are indexed by calculating inverse of its radii and matching it with inter-planar spacing (d) in reciprocal space of XRD data using WinPLOTR software.

High Resolution Transmission Electron Microscopy (HR-TEM)

This technique is the advance version of imaging in TEM, provides the information at atomic scale, with the image of the crystal structure of the sample. The scattered and transmitted beams are used to generate an interference pattern. The phase contrast picture of HRTEM is very small similar to the unit cell in the crystal. It can create images with high resolution below 0.1 \AA magnification. The voltage applied for the electron gun is 200 kV. The well distinguished atomic planes of HRTEM were indexed by calculating the interplanar distance and were compared with the XRD data to confirm the crystal structure.

Samples were prepared by dispersing 1 milligram of MnO_2 powder in 15 ml of ethanol and sonicated in ultrasonicator for homogeneous mixing. A sonicated solution was dropcasted on the commercial TEM grid (carbon coated copper grid). Further, the grid was dried in vacuum oven to evaporate the ethanol for using in TEM.

2.2.6 X-ray Photoelectron Spectroscopy (XPS)

XPS also peculiarly known as electron spectroscopy for chemical analysis (ESCA) is used for the analysis of the chemical state of the elements. This technique is sensitive at the surface which provides knowledge regarding the composition of the materials, oxidation state of the elements constituting the material and valence band structure by probing the surface of the specimen. The principle of XPS is based on the photoelectric effect. When the sample is irradiated with the monochromatic X-ray photons having energy $h\nu$, ejection of electrons takes place from the surface of the sample. Nearby electrons will scatter these photoelectrons, slowing them down and causing them to lose some of their energy. Therefore, photoexcited electrons do not penetrate over the specimen due to high energy loss. This undesirable photoelectron scattering produces unwanted secondary inelastic background intensity. Due to the high degree of scattering, only photoelectrons originating from a depth of a few tens of angstrom can be identified. The kinetic energy (K.E.) of emitted electrons are given by [151]

$$\text{K.E.} = h\nu - \text{B.E.} - \Phi \quad (2.4)$$

where ' $h\nu$ ' represents the energy of the incident X-ray photon, 'B.E.' is the binding energy of the emitted electron and ' Φ ' is the work function. From equation 2.4, it is clear that photoelectrons are produced only if $h\nu \geq \text{B.E.} + \Phi$. The emitted photoelectrons are identified by their respective kinetic energies (KE). Photoelectrons with appropriate KE pass through the work function barrier and reach the detector. In general, when the chamber is evacuated to ultra-high vacuum, scattering and collisions between emitted electrons are reduced. This increases the mean free path of the emitted electrons, allowing them to easily reach the detector. The X-ray photoelectron spectra show the relationship

between the frequencies of emitted electrons and their K.E. The energy distribution of electronic states for a given photon energy is referred to as the distribution of kinetic energy of photoelectrons. In the present study, we employed XPS instrument from VSW Al-K $_{\alpha}$ (energy = 1486.6 eV) radiations. Vacuum level for sample preparation compartment (SPC) was $\sim 10^{-8}$ Torr and the sample analysis chamber (SAC) was $\sim 10^{-9}$ Torr. First of all, we scanned over the full energy range (survey scan), and then specifically selected Mn 2p, O 1s and Dy 3d core level spectra for our study. All observed peaks were calibrated to C 1s peak at ~ 284.6 eV. XPS data were fitted via software XPS peak 4.2 to find out exact peak positions, valance states and area ratio of the elements present in the sample.

2.2.7 Brunauer-Emmett-Teller Measurement (BET)

The standard technique to determine the specific surface area of the sample is done by adsorption of gas. To estimate the surface area Brunauer, Emmett, and Teller (BET) equation is used. Barrett-Joyner-Halenda (BJH) analysis is used to determine the specific pore volume and pore area using a technique performed by adsorption and desorption of the gas. This technique provides both the porosity and pore size distribution of the sample. The parameters like size distribution of the pores, pore shape, particle size along with surface area acts an important position in leading the very important reaction parameters like selectivity, stability and catalytic activity, diffusivity. Specific surface area of the samples was calculated using the data obtained from adsorption at the relative pressure (p/p_0) from 0.05 to 0.35. The sample pore size distribution was calculated from the isotherm curve of desorption using the BJH algorithm. The position of the maximum in the pore-size distribution was defined as pore diameter.

In the present study, Brunauer-Emmett-Teller (BET) surface areas of Dy doped MnO_2 was measured at the temperature $-196\text{ }^\circ\text{C}$ with the help of the Micromeritics ASAP 2020 Analyzer. Under vacuum sample was degassed before the measurement at the temperature $300\text{ }^\circ\text{C}$.

2.2.8 UV-Visible Spectroscopy

UV-Visible spectrophotometer is an optical device used to determine the absorption spectra and the band gap of the materials. In a double beam spectrophotometer, for powder sample, one beam was incident on the sample and other one incident on the standard reference, BaSO_4 powder. To record the spectra a photomultiplier tube (PMT) was used. For the UV light source deuterium lamp was used and for visible light source a tungsten lamp was used.



Figure 2.8: UV-Visible Spectrophotometer.

For powder samples, measurements were carried out in the diffused reflectance mode with the help of an integrating sphere assembly supplied with the Shimadzu 2600 spectrophotometer shown in figure 2.8. Using the Kubelka-Munk function reflectance was converted to the absorbance in the range of 200 to 700 nm.

2.2.9 Magnetic Measurements

Magnetic properties of these material are determined by performing the magnetic measurements of the sample using Magnetic property measurement system (MPMS). The basic measurements are magnetization as a function of temperature at constant magnetic field and magnetization verses applied external magnetic field at a constant temperature. Magnetic Property Measurement System (SQUID, MPMS from Quantum Design, USA (Figure 2.9). This instrument uses vibrating sample magnetometer (VSM) and the superconducting quantum interface device (SQUID) for the measurement of magnetic moment. A concise overview including the working principle of both VSM and SQUID is provided below.

Vibrating sample magnetometer (VSM)

VSM is capable to measure the magnetic moment of the sample with high precession using induction method. This aproach eventually measures the voltage indiced in the series of detection coils when the magnetic moment changes slightly in the sample. In practise, when the sample vibrates vertically with a constant frequency of 60-80 Hz and an amplitude of 1 mm in a uniform magnetic field, the induced voltage at the detection coil can be measured. The DC magnetization measurements of samples are performed in the temperature range of 2 - 300 K. In the beginning, the sample rod is fixed at the center of

the two detection coil with a homogeneous magnetic foeld of ± 7 Tesla. When it is displaced to a certain distance in time, t , the change in flux (ϕ) induces a voltage in the sensing coil given by $v = d\phi/dt$ and is measured in the detection coils. The rate of change of flux is directly the measure of the magnetic moment of the sample. The resulting moment in specimen is then measured with respect to applied magnetic field.



Figure 2.9: MPMS-3, Quantum Design (USA) used for magnetic measurement

SQUID Magnetometer

SQUID magnetometer is one of the most sensitive and effective device to measure the magnetic properties of materials. This is a direct method to measure the magnetic moment of a sample, the device is configured with a magnetometer to detect small magnetic fields. The SQUID magnetometer used in the present work has a highest sensitivity of 5×10^{-8} emu and frequency range of 0.1 Hz - 1 KHz. In this system, direct phase nulling technique measures and cancels background AC phase shifts at every measurement. The rate of change of temperature was 10 K/min from 300 K to 10 K and was 2 K/min from 10 K to 2 K. The frequencies used for the ac susceptibility measurement are 31, 101, 299 and 501 Hz. In all samples real and imaginary parts of susceptibility were measured with varying temperature and keeping frequency constant where magnetic field varies in detection coils.

2.2.10 Electrochemical Measurements

Electrochemical properties of synthesised products are examined using electrochemical workstation (CHI 7044). The electrochemical performances of the prepared materials were studied by executing cyclic voltammetry (CV), Galvanostatic charge/discharge (GCD) and Electrochemical impedance spectroscopy (EIS) measurements using three electrode cell. An electrochemical workstation consists of a potentiostat, relevant control software at one end, and the electrochemical three electrode cell setup at the other end.

In electrochemistry, three-electrode cell is the most common setup used for electrochemical measurements. The three electrodes are working electrode (WE), counter electrode (CE) and reference electrode (RE). These electrodes are immersed in suitable electrolyte as shown in figure 2.10.

1. Counter or auxiliary electrode

A counter electrode serves as a conductor in the electrochemical cell, completing the circuit. The current enters the electrolyte through the working electrode and exits the electrolyte solution through the counter electrode. Counter electrodes are frequently made up of an inert material (such as Pt, Au, etc.) that does not take part in electrochemical reaction, i.e. it is non-reactive in nature. The main requirement of using CR in this process is to provide high surface area. The total surface area of the counter electrode must be greater than that of the working electrode to avoid becoming a limiting factor in the mechanism of the electrochemical method.

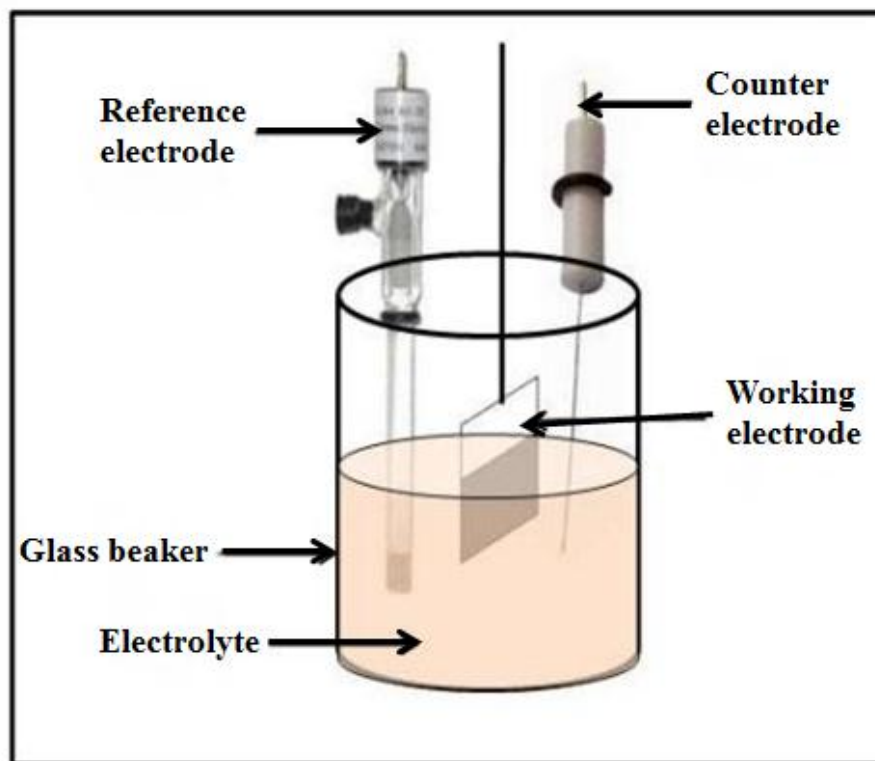


Figure 2.10: An electrochemical three electrode setup.

2. Reference electrode

The reference electrode is an electrode whose potential is well-known and constant. It is used as a reference for measure the potential of working electrode. The high stability of the potential of reference electrode is achieved by using a redox system with saturated concentrations of each participants of the redox reaction. The current flowing through the reference electrode is kept as near to zero as possible. Silver-Silver Chloride (Ag/AgCl) or Saturated Calomel Electrode (SCE) are two often used reference electrodes.

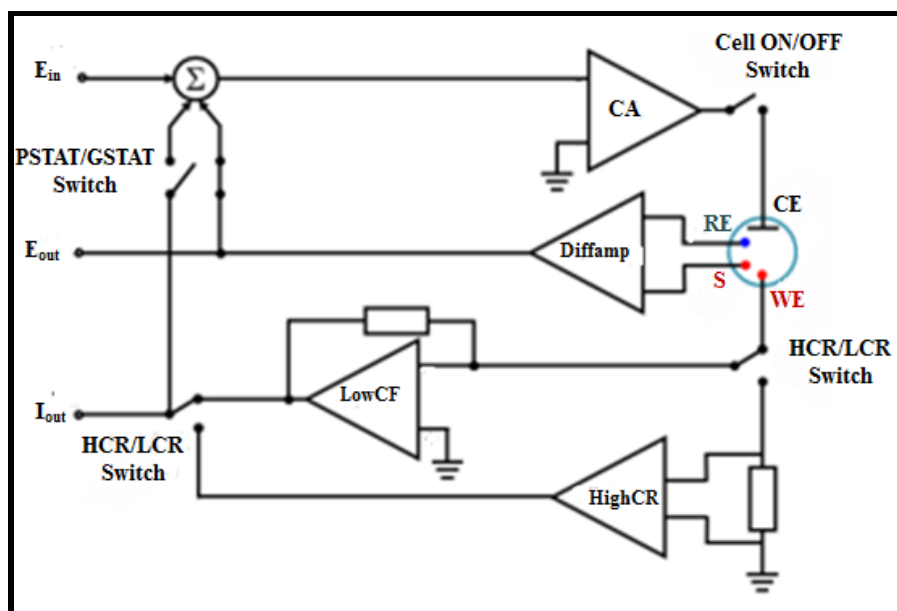


Figure 2.11: Schematic circuit diagram of electrochemical three electrode setup (Potentiostat/Galvanostat, PSTAT/GSTAT).[152]

3. Working electrode

The working electrode provides the surface on which the electrochemical reaction takes place and measure the current with controlled potential. Common electrodes used for the

construction of working electrodes are such as glassy carbon electrode (GCE), Hg drop, toray paper and films etc. The material used as a WE determines the overall performance of a supercapacitor in the supercapacitor application. Current flows inbetween the working electrode and the counter electrode.

The potential difference is regulated between the working electrode and counter electrode and monitored between the reference electrode and S (shown in figure 2.11). The potential difference between reference electrode and working electrode is regulated by controlling the polarization of CE. The potential between the working electrode and counter electrode is the voltage applied by the amplifier. It is adjusted such that the potential difference between the working electrode and reference electrode will be equal to the potential difference quantified by the user. This configuration enables for adjustment of the potential difference across the electrochemical contact at the WE with regard to the RE [152].

Preparation of working electrode

In the present work, we have prepared electrodes by using toray paper and glassy carbon electrode (GCE).

(1) Toray paper

Working electrode was prepared by dispersing fixed amount of bare and Dy doped MnO_2 samples in 150 ml of ethanol. The prepared solution was drop casted over the toray paper without using any carbon additive or binder. The coated area of the electrode was of 1 cm x 1 cm and then dried at 80°C for 12 h in a vacuum oven. The mass of the active material present in the electrode was found to be ~3 mg. Electrochemical analysis was done by performing cyclic voltammetry and charge/ discharge in 1M Na_2SO_4 electrolyte solution in

a potential window of 0 to 0.8 V. Electrochemical impedance spectroscopy was also done to determine the resistance of the materials.

(2) Glassy carbon electrode

Active material was prepared by dissolving 4 mg of prepared sample in 500 μl of ethanol. The solution was sonicated for 15 min and drop casted over glassy carbon electrode. The electrode was dried at room temperature for 15 min. Cyclic voltammetry test was performed in 1M Na_2SO_4 electrolyte solution at room temperature.